NASA

Technical Memorandum 80292

Postseismic Viscoelastic Surface Deformation and Stress
Part 1: Theoretical Considerations, Displacement and Strain Calculations

Steven C. Cohen

(NASA-TM-80292) POSTSEISMIC VISCOELASTIC SURFACE DEFORMATION AND STRESS. PART 1: THEORETICAL CONSIDERATIONS, DISPLACEMENT AND STRAIN CALCULATIONS (NASA) 38 p HC A03/MF A01 CSCL 08K G3/46

N79-28830

Unclas 32223

MAY 1979

National Aeronautics and Space Administration

Goddard Space Flight Center
Greenbelt, Maryland 20771

TM 80292

POSTSEISMIC VISCOELASTIC SURFACE DEFORMATION AND STRESS

Part I: Theoretical Considerations, Displacement and Strain Calculations

Steven C. Cohen
Geodynamics Branch

MAY 1979

GODDARD SPACE FLIGHT CENTER
Greenbelt, Maryland 20771

FIGURE CAPTIONS

Figure 1. Model of a Strike-Slip Fault in a Layer Lying Over a Half-Space.

Figure 2a. Rheological Element for Standard Viscoelastic Solid.
2b. Rheological Element for Maxwell Substance.

Figure 3. Displacements Parallel to the Fault, u(t), for Model DILE; u_0 = 1 m; Tick Mark Spacing = 2L

Figure 4. Displacements Perpendicular to the Fault, v(t), for Model DILE; u_0 = 1 m.

Figure 5. Shear Strain, $\epsilon_{12}(t)$ for Model DILE; u_0 = 1 m.

Figure 6. Normal Strain, $\epsilon_{11}(t)$, for Model DILE; u_0 = 1 m.

Figure 7. Normal Strain, $\epsilon_{22}(t)$, for Model DILE; u_0 = 1 m.

Figure 8. Rotation $\omega(t)$ for Models DILE and DILV; u_0 = 1 m.

Figure 9. Displacements Parallel to the Fault, u(t), for Model DILV; u_0 = 1 m.

Figure 10. Displacements Perpendicular to the Fault, v(t), for Model DILV; u_0 = 1 m.

Figure 11. Shear Strain, $\epsilon_{12}(t)$, for Model DILV; u_0 = 1 m.

Figure 12. Normal Strain, $\epsilon_{11}(t)$, for Model DILV; u_0 = 1 m.

Figure 13. Normal Strain, $\epsilon_{22}(t)$, for Model DILV; u_0 = 1 m.

Figure 14a. Parallel Displacement, u(t), Versus Distance from the Fault for Model DILE; u_0 = 1 m, L = 50 km for the Scales on Top and Right Side of Figure.
14b. Parallel Displacement u(t), Versus Distance from the Fault for Infinite Fault; u_0 = 1 m, H = 50 km for the Scales on Top and Right Side of Figure.

Figure 15a. Shear Strain, $\epsilon_{12}(t)$, Versus Distance from the Fault for Model DILE; u_0 = 1 m, L = 50 km for the Scales on Top and Right Side of Figure.
15b. Shear Strain, $\epsilon_{12}(t)$, Versus Distance from the Fault for Infinite Fault; u_0 = 1 m, L = 50 km for the Scales on Top and Right Side of Figure.

POSTSEISMIC VISCOELASTIC SURFACE DEFORMATION AND STRESS
Part I: Theoretical Considerations, Displacement and Strain Calculations

Steven C. Cohen
Geodynamics Branch
Goddard Space Flight Center
Greenbelt, Maryland 20771

ABSTRACT

This paper, the first of two related articles, presents a model of viscoelastic deformations associated with earthquakes. A strike-slip fault is represented by a rectangular dislocation in a viscoelastic layer (lithosphere) lying over a viscoelastic half-space (asthenosphere). Deformations occur on three time scales. The initial response is governed by the instantaneous elastic properties of the earth. A slower response is associated with viscoelastic relaxation of the lithosphere and a yet slower response is due to viscoelastic relaxation of the asthenosphere. The major conceptual contribution of this paper is the inclusion of lithospheric viscoelastic properties into a dislocation model of earthquake related deformations and stresses. Numerical calculations using typical fault parameters reveal that the postseismic displacements and strains are small compared to the coseismic ones near the fault, but become significant further away. Moreover, the directional sense of the deformations attributable to the elastic response, the lithospheric viscoelastic softening, and the asthenospheric viscoelastic flow may differ and depend on location and model details. The results and theoretical arguments suggest that the stress changes accompanying lithospheric relaxation may also be in a different sense than and be larger than the strain changes.

POSTSEISMIC VISCOELASTIC SURFACE DEFORMATION AND STRESS
Part 1: Theoretical Considerations, Displacement and Strain Calculations

INTRODUCTION

The subject of this study is the spatial and temporal dependence of postseismic displacements, strains, and stresses. In this paper we develop a theoretical model of the postseismic deformations and report on calculations of surface displacements and strains. In a companion paper (Cohen and Cook, to be published), herein referred to as Part 2, we report the corresponding stresses and examine the effects of variation in fault parameters on the computed deformations.

Our analysis is based on a viscoelastic model of the earth's rheology and employs features from dislocation theory (Steketee, 1958a, 1958b; Chinnery, 1961, 1963; Press, 1965; Rybicki, 1971) and the correspondence principle (Flugge, 1967). The assumed model for a strike-slip fault is shown in Figure 1. The lithosphere is modeled as a layer of thickness H lying over an asthenospheric half-space. The strike-slip faulting occurs uniformly over a rectangular surface from -L to L and from some upper level which is not necessarily the surface to a depth D within the lithosphere. As will be seen below, the deformations depend on both the deviatoric and dilatational rheology of the lithosphere and the deviatoric rheology of the asthenosphere. We assume that both the lithosphere and asthenosphere exhibit viscoelastic deviatoric responses although the details of the response and the associated time scales are different. The dilatational response of the lithosphere is taken to be elastic in one version of our model and viscoelastic in another. Specifically we model the lithospheric deviatoric behavior with the standard linear solid shown in Figure 2a. The dilatational response is represented by an elastic element in model DILE and a standard linear solid in model DILV. In the latter case the deviatoric and dilatational time constants are assumed equal. The deviatoric response of the asthenosphere is modeled by a Maxwell element shown in Figure 2b.

The time constants associated with the lithospheric and asthenospheric viscoelasticity are expected to be markedly different. Although there is some debate about the physical mechanism for the lithospheric viscoelasticity we take an empirical approach based on laboratory and field investigations which yield time constants ranging from several minutes to a few months (e.g. Robertson, 1964). On the other hand asthenospheric viscoelasticity has a longer time constant expected to range from years to decades (e.g. Nur and Mavko, 1974), or longer.

Two more preliminary comments need to be made about this model. First the consideration of the lithosphere's dilatational response is important only for finite length faults. For infinitely long faults only the deviatoric behavior has to be considered and the model is two-dimensional. We have already reported some results from this model (Cohen, 1979) and will discuss others below. The present results comprise the more detailed study to which we alluded in the earlier paper. Second, as the thickness of the lithosphere increases (with fault depth held constant), the influence of the asthenosphere decreases. In the limit that the lithosphere becomes infinitely thick, model DILV gives no post-seismic deformations but model DILE does. This general result, based on the correspondence principle, is discussed in many references. Viscoelastic calculations based on an infinite half-space model of the earth have been reported by Singh and Rosenman (1974), and Rosenman and Singh (1973a, 1973b). Models involving dislocation theory and a layer over a half space have been studied by Rundle and Jackson (1977), Savage and Prescott (1978), and Rundle (1978). A viscoelastic model of the Palmdale bulge has recently been reported by Rundle and Thatcher (1979).

THEORETICAL CONSIDERATIONS

The starting point for our analysis is the set of equations describing the static displacements associated with a dislocation in an elastic layer lying over an elastic half-space. A set of approximate equations have been derived using an image technique by Rundle and Jackson (1977) who find

$$4\pi \frac{u}{u_0} = \left\{ y\,t\,\alpha \left[\frac{1}{S_1\,(S_1+q)} + \frac{(1+c)\,S_2 + (1-b)\,p + q}{S_2\,(S_2+p)^2} - \frac{(p^2-q^2)\,(2S_2+p)}{2S_2^{\,3}\,(S_2+p)^2} \right] \right.$$

$$+ \tan^{-1}\frac{qt}{yS_1} + \tan^{-1}\frac{pt}{yS_2} + \sum_{m=1}^{\infty}\left(\frac{\mu_1-\mu_2}{\mu_2+\mu_2}\right)^m \left\{ y\,t\,\alpha \left[\frac{1}{S_{1_+}(S_{1_+}+q_+)} \right.\right.$$

$$\left.\left. + \frac{(1+c)\,S_{2_+} + (1-b)p_+ + q_+}{S_{2_+}\,(S_{2_+}+p_+)^2} - \frac{(p_+^{\,2}-q_+^{\,2})\,(2S_{2_+}+p_+)}{2S_{2_+}^{\,3}\,(S_{2_+}+p_+)^2} \right] + \tan^{-1}\frac{q_+ t}{yS_{1_+}} \right. \qquad (1)$$

$$+ \tan^{-1}\frac{p_+ t}{yS_{2_+}} + y\,t\,\alpha \left[\frac{1}{S_{2_-}\,(S_{2_-}+q_-)} + \frac{(1+c)\,S_{2_-} + (1-b)\,p_- + q_-}{S_{2_-}\,(S_{2_-}+p_-)^2} \right.$$

$$\left.\left.\left. - \frac{(p_-^{\,2}-q_-^{\,2})\,(2S_{2_-}+p_-)}{2\,S_{2_-}^{\,3}\,(S_{2_-}+p_-)^2} \right] + \tan^{-1}\frac{q_- t}{yS_{1_-}} + \tan^{-1}\frac{q_- t}{yS_{2_-}} \right\}\right\}\right|$$

and

$$4\pi \frac{v}{u_0} = \left\{ (1-\alpha)\,\ell n\,(S_1+q) + (1-\alpha-\alpha c)\,\ell n\,(S_2+p) - \alpha \left[\frac{(b+c)p-q}{S_2+p} + \frac{(p^2-q^2)}{2\,S_2\,(S_2+p)} \right] \right.$$

$$- y^2\,\alpha \left[\frac{1}{S_1\,(S_1+q)} + \frac{(1-c)\,S_2 + (1-b)\,p + q}{S_2\,(S_2+p)^2} - \frac{(p^2-q^2)\,(2S_2+p)}{2S_2^{\,3}\,(S_2+p)^2} \right]$$

$$+ \sum_{m=1}^{\infty}\left(\frac{\mu_1-\mu_2}{\mu_1+\mu_2}\right)^m \left\{ (1-\alpha)\,\ell n\,(S_{1_+}+q_+) + (1-\alpha-\alpha c)\,\ell n\,(S_{2_+}+p_+) \right. \qquad (2)$$

$$- \alpha \left[\frac{(b+c)p_+ - q_+}{S_{2_+}+p_+} + \frac{(p_+^{\,2}-q_+^{\,2})}{2S_{2_+}\,(S_{2_+}+p_+)} \right] - y^2\,\alpha \left[\frac{1}{S_{1_+}\,(S_{1_+}+q_+)} \right.$$

$$\left.\left. + \frac{(1+c)\,S_{2_+}\,(1-b)p_+ + q_+}{S_{2_+}\,(S_{2_+}+p_+)^2} - \frac{(p_+^{\,2}-q_+^{\,2})\,(2S_{2_+}+p_+)}{2S_{2_+}^{\,3}(2S_{2_+}+p_+)} \right] + (1-\alpha)\,\ell n(S_{1_-}+q_-) \right.$$

$$+ (1 - \alpha - \alpha c) \ell n (S_{2\_} + p_{\_}) - \alpha \left[\frac{(b + c)\, p_{\_} - q_{\_}}{S_{2+} + p_{\_}} + \frac{(p_{\_}^2 - q_{\_}^2)}{2\, S_{2\_} (S_{1\_} + p_{\_})} \right]$$

(2)

$$- y^2 \alpha \left[\frac{1}{S_{1\_} (S_{1\_} + q_{\_})} + \frac{(1 + c)\, S_{2\_} + (1 - b)\, p_{\_} + q_{\_}}{(S_{2\_} + p_{\_})^2} - \frac{(p_{\_}^2 - q_{\_}^2)\, (2 S_{2\_} + p_{\_})}{2 S_{2\_}^3 (S_{2\_} + p_{\_})^2} \right] \Bigg\} \Bigg|$$

where the symbols used in these equations are defined on Table I and where (Chinnery, 1961, 1963)

$$f(\eta, \zeta) \Big|\Big| = f(L, D) - f(L, d) - f(-L, D) + f(-L, d) \tag{3}$$

In order to find the corresponding time dependent viscoelastic displacements we can follow the procedure dictated by the correspondence principle. We write the stress-strain equations for the viscoelastic material as

$$P\sigma = Q\epsilon \tag{4}$$

where P and Q are linear operators. For the case of pure elasticity, P = 1 and Q = 3k or Q = 2μ depending on whether dilatational or deviatoric behavior is under study. In the more general case when P and Q are linear operators we take the Laplace transform of equation 4 to find

$$P(s)\, \overline{\sigma} = Q(s)\, \overline{\epsilon} \tag{5}$$

where P and Q are polynomials in the Laplace transform variable s. Equation 5 shows that the Laplace transformed viscoelastic solution can be obtained from the elastic solution by making the substitutions

$$3k \rightarrow \frac{P(s)}{Q(s)} \quad ; \quad \text{dilatational case} \tag{6a}$$

and

$$2\mu \rightarrow \frac{P(s)}{Q(s)} \quad ; \quad \text{deviatoric case} \tag{6b}$$

It is also necessary to include the transformation

$$\bar{u}_0 = \frac{u_0}{s} \quad \text{since } u_0 = \text{a constant for } t > 0 \tag{7}$$

The resulting equations for u and v can then be subject to an inverse transformation to determine the viscoelastic displacements. This procedure is very cumbersome. A more expeditious procedure results from two simplifications. First we impose the physically reasonable condition that the lithosphere relaxes rapidly compared to the asthenosphere. Next we restrict the discussion to the three times of greatest interest, namely, $t = t_0 = 0$ – the time immediately after the earthquake, $t = t_\ell$ – a time long compared to that required for lithospheric relaxation, and $t = t_a$ – a time long compared to that required for asthenospheric relaxation. In these three time limits the displacement equations become elastic with effective reduced moduli μ_1, μ_2, and k as shown on Table II. The parameter substitutions shown on Table II are obtained directly from consideration of the viscoelastic stress–strain equations. Consider, for example, the deviatoric equation for a three element standard linear solid

$$\sigma + \frac{\eta}{\mu_a + \mu_b} \dot{\sigma} = \frac{\mu_a \mu_b}{\mu_a + \mu_b} \epsilon + \frac{\eta \mu_a}{\mu_a + \mu_b} \dot{\epsilon} \tag{8}$$

For a rapid change in stress and strain (e.g. during an earthquake) the terms in $\dot{\sigma}$ and $\dot{\epsilon}$ dominate so

$$\Delta\sigma = \mu_a \, \Delta\epsilon \tag{9}$$

while for $\dot{\sigma}$ and $\dot{\epsilon}$ small

$$\sigma = \frac{\mu_a}{1+\beta} \epsilon, \; \beta = \frac{\mu_a}{\mu_b} \tag{10}$$

For a Maxwell substance

$$\sigma + \frac{\eta}{\mu} \dot{\sigma} = \eta \dot{\epsilon} \tag{11}$$

Thus for rapid changes

$$\Delta\sigma = \mu \Delta\epsilon \tag{12}$$

while for $\dot{\sigma}$ and $\dot{e}$ small

$$\sigma = 0 \tag{13}$$

The two viscoelastic models that we have considered have in common the standard linear solid representation of the deviatoric behavior of the lithosphere and the Maxwell deviatoric behavior of the asthenosphere. They differ in that model DILE takes the lithosphere to be elastic in dilatation and model DILV takes to be a standard solid with $\mu_a/\mu_b = k_a/k_b$ and $\eta/\mu_b = \eta'/k_b$. The displacements at the earth's surface ($z = 0$) are in these models:

$$\begin{aligned} 4\pi \frac{u}{u_0} = \Bigg\{ & a_1 \frac{y\,t}{S\,(S+p)} + a_2 \frac{y\,t}{(S+p)^2} + a_3 \frac{y\,t\,p}{S\,(S+p)^2} + a_4 \tan^{-1} \frac{t\,p}{yS} \\ & + \sum_{m=1}^{\infty} \Gamma^m \Bigg[a_5 \frac{y\,t}{S_1\,(S_1+q_+)} + a_6 \frac{y\,t}{(S_2+p_+)^2} + a_7 \frac{y\,t\,p_+}{S_2\,(S_2+p_+)^2} \\ & + a_8 \frac{y\,t\,q_+}{S_2\,(S_2+p_+)^2} + a_9 \frac{4\,y\,t\,\zeta\,H\,m\,(2\,S_2+p_+)}{S_2^{\,3}\,(S_2+p_+)^2} \\ & + a_{10} \tan^{-1} \frac{q_+ t}{y S_1} + a_{11} \tan^{-1} \frac{p_+ t}{y S_2} \Bigg] \Bigg\} \end{aligned} \tag{14}$$

and

$$\begin{aligned} 4\pi \frac{v}{u_0} = \Bigg\{ & b_1 \frac{y}{S\,(S+p)} + b_2 \frac{p}{S+p} + b_3 \frac{y^2}{S\,(S+p)} + b_4 \left(\frac{y}{S+p} \right)^2 \\ & + b_5 \frac{p\,y^2}{S\,(S+p)^2} + \sum_{m=1}^{\infty} \Gamma^m \Bigg[b_6 \ln (S_1+q_+) + b_7 \ln (S_2+p_+) \\ & + b_8 \frac{p_+}{S_2+p_+} + b_9 \frac{q_+}{S_2+p_+} + b_{10} \frac{4\,\zeta\,H\,m}{S_2\,(S_2+p_+)} \\ & + b_{11} \frac{y^2}{S_1\,(S_1+q_+)} + b_{12} \left(\frac{y}{S_2+p_+} \right)^2 + b_{13} \frac{y^2\,p_+}{S_2\,(S_2+p_+)^2} \end{aligned} \tag{15}$$

$$+ b_{14} \frac{y^2 q_+}{S_2 (S_2 + p_+)^2} + b_{15} \frac{4 y^2 \zeta H m y^2 (2 S_2 + p_+)}{S_2^3 (S_2 + p_+)^2} \Bigg] \Bigg\} \Bigg\| \tag{15}$$

where the coefficients a_i and b_i depend on time and the model; they are shown on Table III. The time dependent quantity Γ has been evaluated in an earlier paper (Cohen, 1979) and is given by

$$\Gamma(t_0) = \frac{\gamma - 1}{\gamma + 1} \tag{16a}$$

$$\Gamma(t_\beta) = \frac{\gamma - 1 - \beta}{\gamma + 1 + \beta} \tag{16b}$$

$$\Gamma(t_a) = 1 \tag{16c}$$

where $\gamma = \mu_a/\mu$ and as before $\beta = \mu_a/\mu_b$.

The strains are obtained from appropriate differentiations on the displacements:

$$\frac{4\pi}{u_0} \frac{\partial u}{\partial x} = 4\pi \frac{\epsilon_{11}}{u_0} = \Bigg\{ a_1 \frac{y[t^2 (2S + p) - S^2 (S + p)]}{S^3 (S + p)^2} + a_2 \frac{y[2t^2 - S (S + p)]}{S (S + p)^3}$$

$$+ a_3 \frac{y p[t^2 (3S + p) - S^2 (S + p)]}{S^3 (S + p)^2} + a_4 \frac{y p (t^2 - S^2)}{S [y^2 S^2 + p^2 t^2]}$$

$$+ \sum_{m=1}^{\infty} \Gamma^m \Bigg\{ a_5 y \left[\frac{t^2 (2S_1 + q_+) - S_1^2 (S_1 + q_+)}{S_1^3 (S_1 + q_+)}\right] + a_6 y \left[\frac{2t^2 - S_2 (S_2 + p_+)}{S_2 (S_2 + p_+)^3}\right] \tag{17}$$

$$+ a_7 y p_+ \left[\frac{t^2 (3S_2 + p_+) - S_2^2 (S_2 + p_+)}{S_2 (S_2 + p_+)^3}\right] + a_8 y q_+ \left[\frac{t^3 (3S_2 + p_+) - S_2^2 (S_2 + p_+)}{S_2 (S_2 + p_+)^3}\right]$$

$$+ a_9 4 y H \zeta m \left[\frac{t^2 (2S_2 + p_+)(5S_2 + 3p_+) - S_2 (S_2 + p_+)[S_2 (S_2 + p_+) + 2t^2]}{S_2^5 (S_1 + p_+)^3}\right]$$

$$+ a_{10} \frac{y q_+ (t^2 - S_1^2)}{S_1 (S_1^2 y^2 + q_+^2 t^2} + a_{11} \frac{y p_+ (t^2 - S_2^2)}{S_2 (S_2^2 y^2 + p_+^2 t^2)} \Bigg\} \Bigg\} \Bigg\|$$

and

$$\frac{4\pi}{u_0}\frac{\partial v}{\partial y} = \frac{4\pi}{u_0}\epsilon_{22} = \Bigg\{ b_1 \frac{y}{S(S+p)} + b_2\left[\frac{-y\,p}{S(S+p)}\right] + b_3\, y\left[\frac{2S^2(S+p)-y^2(2S+p)}{S^3(S+p)^2}\right]$$

$$+ b_4\, 2y\left[\frac{S(S+p)-y^2}{S(S+p)^3}\right] + b_5\, y\, p\left[\frac{2S^2(S+p)-y^2(3S+p)}{S^3(S+p)^3}\right]$$

$$+ b_6 \frac{y}{S_1(S_1+p)} + b_7 \frac{y}{S_2(S_2+p_+)} + b_8\left[\frac{-y\,p_+}{S_2(S_2+p_+)^2}\right]$$

$$+ b_9\left[\frac{-y\,q_+}{S_2(S_2+p_+)^2}\right] + b_{10}\left[\frac{-4\,y\,H\zeta\,m(2S_2+p_+)}{S_2{}^3(S_2+p_+)^2}\right] \qquad (18)$$

$$+ b_{11}\, y\left[\frac{2S_1{}^2(S_1+q_+)-y^2(2S_1+q_+)}{S_1{}^3(S_1+q_+)^2}\right] + b_{12}\, 2y\left[\frac{S_2(S_2+p_+)-y^2}{S_2(S_2+p_+)^3}\right]$$

$$+ b_{13}\, yp_+\left[\frac{2S_2(S_2+p_+)-y^2(3S_2+p_+)}{(S_2(S_2+p_+))^3}\right] + b_{14}\, yq_+\left[\frac{2S_2(S_2+p_+)-y^2(3S_2+p_+)}{(S_2(S_2+p_+))^3}\right]$$

$$+ b_{15}\, 4\,y\,H\zeta\,m\left[\frac{2S_2(S_2+p_+)[S_2(2S_2+p_+)+y^2]-y^2(2S_2+p_+)(5S_2+3p_+)}{S_2{}^5(S_2+p_+)^3}\right]\Bigg\}\Bigg\}\Bigg\}$$

and

$$\frac{4\pi}{u_0}\frac{\partial u}{\partial y} = \Bigg\{ a_1\, t\left[\frac{S^2(S+p)-y^2(2S+p)}{S^3(S+p)^2}\right] + a_2\, t\left[\frac{S(S+p)-2y^2}{S(S+p)^3}\right]$$

$$+ a_3\, t\,p\left[\frac{S^2(S+p)-y^2(3S+p)}{(S(S+p))^3}\right] + a_4\left[\frac{-tp(S^2+y^2)}{S(y^2S^2+p^2t^2)}\right] \qquad (19)$$

$$+ \sum_{m=1}^{\infty}\Gamma^m\Bigg\{ a_5\, t\left[\frac{S_1{}^2(S_1+q_+)-y^2(2S_1+q_+)}{S_1{}^3(S_1+q_+)^2}\right] + a_6\, t\left[\frac{S_1(S_1+p_+)-2y^2}{S_2(S_2+p_+)^3}\right]$$

$$+ a_7\, tp_+\left[\frac{S_2{}^2(S_2+p_+)-y^2(3S_2+p_+)}{(S_2(S_2+p_+))^3}\right] + a_8\, tq_+\left[\frac{S_2{}^2(S_2+p_+)-y^2(3S_2+p_+)}{(S_2(S_2+p_+))^3}\right]$$

$$+ a_9\frac{4ytH\zeta m(2S_2+p_+)}{S_2{}^3(S_2+p_+)^2} + a_{10}\left[\frac{-q_+t(S_1{}^2+y^2)}{S_1(y^2S_1{}^2+q_+{}^2t^2}\right] + a_{11}\,tq\left[\frac{-p_+t(S_2{}^2+y^2)}{S_2(y^2S_2{}^2+p_+{}^2t^2)}\right]\Bigg\}\Bigg\}\Bigg\}$$

$$\frac{4\pi}{u_0}\frac{\partial v}{\partial x} = \left\{ b_1\left[\frac{-t}{S(S+p)}\right] + b_2\left[\frac{tp}{S(S+p)^2}\right] + b_3\left[\frac{y^2 t(2S+p)}{S^3(S+p)^2}\right] + b_4\left[\frac{2y^2 t}{S(S+p)^3}\right]\right.$$

$$+ b_5\left[\frac{y^2 tp(3S+p)}{(S(S+p))^3}\right] + \sum_{m=1}^{\infty}\Gamma^m\left\{ b_6\left[\frac{-t}{S_1(S_1+q_+)}\right] + b_7\left[\frac{-t}{S_2(S_2+p_+)}\right]\right.$$

$$+ b_8\left[\frac{tp_+}{S_2(S_2+p_+)^2}\right] + b_9\left[\frac{tq_+}{S_2(S_2+p_+)^2}\right] + b_{10}\left[\frac{4tH\zeta m(2S_2+p_+)}{S_2^3(S_2+p_+)^2}\right] \quad (20)$$

$$+ b_{11}\left[\frac{y^2 t(2S_1+q_+)}{S_1^3(S_1+q_+)}\right] + b_{12}\left[\frac{2y^2 t}{S_2(S_2+p_+)}\right] + b_{13}\left[\frac{-y^2 tp_+(3S_2+p_+)}{(S_2(S_2+p_+))^3}\right]$$

$$\left.\left.+ b_{14}\left[\frac{y^2 tq_+(3S_2+p_+)}{(S_2(S_2+p_+))^3}\right] + b_{15}\,4y^2 tH\zeta m\left[\frac{(2S_2+p_+)(5S_2+3p_+)-2S_2(S_-+p_+)}{S_2^5(S_2+p_+)^3}\right]\right\}\right\}$$

From these we obtain the shear strain

$$\epsilon_{12} = \tfrac{1}{2}\left(\frac{\partial u}{\partial y} + \frac{\partial v}{\partial x}\right) \quad (21)$$

and rotation

$$\omega = -\tfrac{1}{2}\left(\frac{\partial u}{\partial y} - \frac{\partial v}{\partial x}\right) \quad (22)$$

The elastic displacements and strains depend on the location (x, y), the source parameters (ΔU, D, L, H) and the ratio of elastic constants k (or k_a) to μ_a and μ_a to μ. It is convenient to choose as a unit of spatial measurement the half-fault length, L, and to normalize the results to a unit dislocation, ΔU. Furthermore as is common in theoretical geophysics we take the instantaneous) Poisson's ratio to be ¼ corresponding to $\frac{k_1(t_0)}{\mu_1(t_0)} = \frac{5}{3}$ and set $\mu_1(t_0) = \mu_2(t_0)$. This leaves as parameters the quantities D/L and H/L and the coordinates x/L and y/L. The choice of equal instantaneous shear moduli for the lithosphere and asthenosphere sets $\Gamma(t_0) = 0$ and all terms under the summation signs in equations 14, 15, and 17–20 vanish in the calculation of the initial elastic deformations. The deformations associated with the lithospheric relaxations depend on the parameter β of the relaxed standard solid and the parameter $\Gamma(t_0)$ which compares the

effective moduli of the lithosphere and asthenosphere. The deformations occuring as the asthenosphere relaxes are independent of the asthenospheric modulus as this half-space has no long-term rigidity.

We will defer until part 2 a detailed discussion of the stresses that accompany these deformations. However it is worth noting that the surface stresses may have significantly different time histories from the strains. For example, the shear stress, σ_{12}, is given by

$$\sigma_{12}(t_0) = \mu_a \epsilon_{12}(t_0) \tag{22a}$$

$$\sigma_{12}(t_\ell) = \frac{\mu_a}{1+\beta} \epsilon_{12}(t_\ell) \tag{22b}$$

$$\sigma_{12}(t_a) = \frac{\mu_a}{1+\beta} \epsilon_{12}(t_a) \tag{22c}$$

As time progresses from t_0 to t_ℓ not only does the strain change, but so does the effective shear modulus coupling the stress to the strain. Since the fractional change in ϵ_{12} is small in many cases and since β may have a value of order unity, the modulus change can dominate the early postseismic stress history. In fact the reduction in the effective shear modulus causes a decrease in the initial shear stress drop associated with the earthquake. As a consequence there is a partial stress recovery at some points even though the strain undergoes a postseismic decrease. A similar effect has been seen sliding block models of earthquakes that use standard linear solid viscoelastic elements (Dieterich, 1972; Cohen, 1978).

RESULTS

In this section we will discuss some figures which illustrate the deformations predicted by the equations presented above. For this discussion we have chosen the numerical parameters such that $L = H = 4D = 1$ and we have set $d = 0$. In part 2 we consider in more detail the dependence of the deformation properties on the fault parameters. In order to appreciate the magnitude of

deformations it will occassionally be convenient to set 2L = 100 km and to set u_0 = 1 m although scaling to other values of L and u_0 is straight forward. We will also have occasion to compare the present results with those obtained for an infinitely long screw dislocation (Cohen, 1979). Here we again take H = 4D = 50 km but now, of course, L = ∞. The illustrative discussion is for model DILE. For the sake of brevity we will not explicitly discuss the results for model DILV although the relevant contours of displacements and strains will be presented. We warn the reader that the results for our two models are often very different as the postseismic relaxation proceeds. We have chosen to concentrate on model DILE since at least some materials appear to remain dilatationally elastic even when deviatorically viscoelastic.

Contours of equal displacements for DILE are shown in Figures 3 and 4. Strain contours are presented on Figures 5 through 7 and the rotations on Figure 8. The corresponding results for DILV are shown on Figures 9 through 13. (The rotations are the same in the two models.)

A useful way to begin the interpretation of these results is to consider the variation of displacement, u, and shear strain, ϵ_{12}, with distance from the fault along the y axis. Along this axis the effects of the fault edge are least noticeable and in fact v, ϵ_{11}, and ϵ_{22} which depend on finite fault sizes for their existence vanish when x = 0. Even on the y axis, however, some effects of finite fault sizes will be seen at distant points from the fault. Figure 14 shows the expected monotonic decrease in displacement with distance from the fault. The lithospheric relaxation reduces the displacements with the maximum change occurring between y = 25 km and y = 50 km. The asthenospheric relaxation produces an opposite postseismic motion which increases the displacement. The net effect of both relaxations is to produce a maximum forward postseismic displacement of about 3 mm near y = 25 km and a maximum reverse displacement of about 1 mm over a wide zone near, say, y = 175 km. A comparison of these results with

those for the infinite fault can be carried out with the aid of Figure 14b. As expected for fixed H and D the displacements at distant points from the fault are larger when L is infinite. Furthermore, the displacements induced by asthenospheric relaxation become significant relative to the coseismic ones at points closer to the fault when the finite fault size is considered.

The postseismic displacements off the y axis are complex, particularly near the fault edges where there is a convergence of contour lines. One curious feature associated with the lithospheric relaxation is a small region of increased displacements beyond the fault edge.

Returning again to the y axis and examining Figure 15 we find that the shear strain drop is about 10^{-5} at the fault, falls to zero near 40 kilometers, and then becomes positive taking on a value of a few parts in 10^8 year near y=70 km, before decreasing. This reversal in the sign of the shear strain is a clear demonstration of the importance of fault finite size. For an infinite fault only the term $\frac{\partial u}{\partial y}$ contributes to the shear strain. Since u decreases monotonically with distance from the fault the shear strain is always negative. In the finite fault model the term $\frac{\partial v}{\partial x}$ must also be considered. It can become the dominate term at certain points not too close to the fault and produce a positive shear strain. As for the postseismic strain, the lithospheric relaxation reduces the strain near the fault. At more distant points the postseismic strain is positive and at still more distant points it becomes negative again. These strain changes are fractionally small near the fault but significant in regions where the coseismic strain vanishes. The asthenospheric relaxation produces a broad region of strain increase.

Leaving the y axis the behavior of the postseismic strain is complex with regions of both positive and negative strain changes apparent. Lithospheric relaxation produces a small shear strain increase along the x axis near the fault and beyond $|x| = L$. Conversely, there is a strain decrease in a region between the x and y axes. The asthenospheric relaxation decreases the

shear strain near the fault and along both coordinate axes but increases it at some distant points between axes.

The perpendicular displacements, v, and the normal strains ϵ_{11} and ϵ_{22} share the common feature of being focussed on the edges of the slipped region. The v displacements tend to decrease as the lithosphere relaxes although Figure 4 does reveal a region of increased displacement. The asthenospheric adjustment increases the displacements. The net postseismic motion is a decreased displacement near the fault and an increased displacement at distant points.

The normal strains can involve shortening or extension depending on location. The previously observed general tendency for lithospheric relaxation to bring contours closer together and for asthenospheric relaxation to separate them can be observed for these strains. When the postseismic behavior is examined in more detail close to the fault we find that the initial change in ϵ_{11} is a shortening (in the first quadrant). As the asthenosphere relaxes there is an extension but the net motion remains a shortening. The postseismic behavior of ϵ_{22} near the fault is an extension both as the lithosphere and asthenosphere relax. We should re-emphasize that the results presented here are for the case L = H = 4D. An analysis of the dependence of the time dependent deformations on the choice of fault parameters will be included in Part 2.

SUMMARY

This paper has considered lithospheric and asthenospheric viscoelasticity as causes of postseismic surface deformations. Displacement and strain equations have been derived for a strike-slip fault and illustrated for a particular case involving a moderately shallow fault that cuts the surface, a somewhat deeper asthenosphere-lithosphere interface, and a finite fault length. The calculations suggest that near the fault the postseismic deformations are significant for moderate and large earthquakes although the deformations are only a small fraction of the coseismic ones. At various points away

from the fault, the deformations produced by lithospheric relaxation exceed the coseismic deformations; furthermore, over broad distant regions the slower deformations produced by asthenospheric relaxation also exceed the coseismic ones. The sense of direction of these postseismic motions not only differs from the sense of the coseismic motions but also varies with location and time.

Accompanying the postseismic changes in strain are changes in stress. However, as the lithosphere relaxes or softens the reduction in its effective moduli causes stress changes that may be very much different from that expected from strain changes alone. The time-dependent changes in stress will be studied in detail in Part 2.

We wish to emphasize that we do not regard viscoelastic motions as the only possible source of postseismic deformations. Other factors, such as postseismic fault creep and time-dependent rock failure, may be important sources of deformation.

ACKNOWLEDGMENT

Glenn Cook provided assistance in the computer programming aspects of this work and was responsible for generating the contour plots.

REFERENCES

Chinnery, M.A., "The Deformation of the Ground Around Surface Faults," Bull. Seismol, Soc. Am., 51, 355-372, 1961.

Chinnery, M.A., "The Stress Changes that Accompany Strike-Slip Faulting," Bull. Seismol. Soc. Am., 53, 921-932, 1963.

Cohen, S. C., "The Viscoelastic Stiffness Model of Seismicity," J. Geophys. Res., 83, 5425-5431, 1978.

Cohen, S.C., "Postseismic Surface Deformations Due to Lithospheric and Asthenospheric Viscoelasticity," Geophys. Res. Letters, 6, 129-131, 1979.

Dieterich, J.H., "Time Dependent Friction as a Possible Mechanism for Aftershocks," J. Geophys. Res. 77, 3771-3781, 1972.

Flugge, W., Viscoelasticity, Blaisdell, Waltham, Mass., 1967.

Nur, A. and G. Mavko, "Postseismic Viscoelastic Rebound," Science, 183, 204-206, 1974.

Press, F., "Displacements, Strains, and Tilts at Teleseismic Distances," J. Geophys. Res., 70, 2395-2412, 1965.

Robertson, E.C., "Viscoelasticity of Rocks," State of Stress in the Earth's Crust, W.R. Judd (Ed.), Elsevier, New York, 1964.

Rosenman, M. and S. J. Singh, "Quasi-Static Strain and Tilts Due to Faulting in a Viscoelastic Half-Space," Bull. Seism. Soc. Am., 63, 1737-1752, 1973a.

Rosenman, M. and S. J. Singh, "Stress Relaxation in a Semi-Infinite Viscoelastic Earth Model," Bull. Seism. Soc. Am., 63, 2145-2154, 1973b.

Rundle, J.B., "Viscoelastic Crustal Deformation by Finite Quasi-Static Sources," J. Geophys. Res., 83, 5937-5945, 1978.

Rundle, J.B. and D.D. Jackson, "A Three-Dimensional Viscoelastic Model of a Strike-Slip Fault," Geophys. J.R. Astr. Soc., 49, 565-591, 1977.

Rundle, J.B. and W. Thatcher, "On Crustal Stress Relaxation and the Palmdale Uplift," Trans. Am. Geophys. U., 59, 1206, 1978.

Rybicki, K., "The Elastic Residual Field of a Very Long Strike-Slip Fault in the Presence of a Discontinuity," Bull. Seism. Soc. Am., 61, 79-92, 1971.

Savage, J.C. and W. H. Prescott, "Asthenospheric Readjustment and the Earthquake Cycle," J. Geophys. Res., 83, 3369-3376, 1978.

Singh, S.J. and M. Rosenman, "Quasi-static Deformation of a Viscoelastic Half-Space by a Displacement Dislocation," Phys. Earth. Planet. Int., 8, 87-101, 1974.

Steketee, J.A., "On Volterra's Dislocations in a Semi-Infinite Medium," Can. Jour. Phys., 36, 192-205, 1958a.

Stekette, J.A., "Some Geophysical Applications of the Elasticity Theory of Dislocations," Can. Jour. Phys., 36, 1168-1197, 1958b.

Table I
Symbol Definition for Displacement and Strain Equations

x, y, z		coordinates of observation point
$\xi, 0, \zeta$		coordinates of a point on the fault
L		half-fault length = $2L$ $\quad -L \leqslant \zeta \leqslant L$
D		depth of lower boundary of fault $\quad d \leqslant \zeta \leqslant D$
d		depth of upper boundary of fault
H		depth to lithosphere-asthenosphere boundary
p	$=$	$\zeta + z$
q	$=$	$\zeta - z$ — for $z = 0$, $p = q$
p_+	$=$	$\zeta + z + 2mH$
p_-	$=$	$\zeta - z + 2mH$ — for $z = 0$, $p_+ = p_-$
q_+	$=$	$\zeta - z - 2mH$
q_-	$=$	$\zeta + z + 2mH$ — for $z = 0$, $q_+ = q_-$
t	$=$	$\xi - x$
S_1^2	$=$	$t^2 + y^2 + q^2$
S_2^2	$=$	$t^2 + y^2 + p^2$ — for $z = 0$, $S_1 = S_1 = S$
$S_{1_+}^2$	$=$	$t^2 + y^2 + q_+^2$
$S_{1_-}^2$	$=$	$t^2 + y^2 + q_-^2$ — for $z = 0$, $S_{1_+} = S_{1_-} = S_1$
$S_{2_+}^2$	$=$	$t^2 + y^2 + p_+^2$
$S_{2_-}^2$	$=$	$t^2 + y^2 + p_-^2$ — for $z = 0$, $S_{2_+} = S_{2_-} = S_1$
u		displacement parallel to fault
u_0		dislocation across fault
v		displacement perpendicular to fault
k_1	$=$	bulk modulus of lithosphere
μ_1	$=$	shear modulus of lithosphere
μ_2	$=$	shear modulus of asthenosphere
α	$=$	$(3k_1 + \mu_1)/(3k_1 + 4\mu_1)$
b	$=$	$(3k_1 - \mu_1)/(3k_1 + \mu_1)$
c	$=$	$3\mu_1 (3k_1 - 2\mu_1)/(3k_1 + \mu_1)$

Table II
Effective Moduli of Lithosphere and Asthenosphere

	Model DILE			Model DILV		
time / modulus	0	t_ℓ	t_a	0	t_ℓ	t_a
μ_1	$\frac{\mu_a}{2}$	$\frac{\mu_a}{2}\frac{1}{1+\beta}$	$\frac{\mu_a}{2}\frac{1}{1+\beta}$	$\frac{\mu_a}{2}$	$\frac{\mu_a}{2}\frac{1}{1+\beta}$	$\frac{\mu_a}{2}\frac{1}{1+\beta}$
k_1	$\frac{k_a}{3}$	$\frac{k_a}{3}$	$\frac{k_a}{3}$	$\frac{k_a}{3}$	$\frac{k_a}{3}\frac{1}{1+\beta}$	$\frac{k_a}{3}\frac{1}{1+\beta}$
μ_2	$\frac{\mu}{2}$	$\frac{\mu}{2}$	0	$\frac{\mu}{2}$	$\frac{\mu}{2}$	0

Table III

Coefficient in Displacement and Strain Equations; Equations 14, 15, 17--20; $\kappa = \frac{k_1}{\mu_1}$

$a_1 : \frac{3\kappa + 1}{3\kappa + 4}$	$b_1 : \frac{3}{3\kappa + 1}$
$a_2 : \frac{9\kappa^2 + 15\kappa - 5}{(3\kappa + 1)(3\kappa + 4)}$	$b_2 : \frac{3}{3\kappa + 1}$
$a_3 : \frac{3\kappa + 7}{3\kappa + 4}$	$b_3 : -\frac{3\kappa + 1}{3\kappa + 4}$
$a_4 : 2$	$b_4 : -\frac{9\kappa^2 + 15\kappa - 5}{(3\kappa + 1)(3\kappa + 4)}$
$a_5 : \frac{6\kappa + 2}{3\kappa + 4}$	$b_5 : -\frac{3\kappa + 7}{3\kappa + 4}$
$a_6 : \frac{18\kappa^2 + 30\kappa - 10}{(3\kappa + 1)(3\kappa + 4)}$	$b_6 : \frac{6}{3\kappa + 4}$
$a_7 : \frac{12}{3\kappa + 4}$	$b_7 : \frac{18}{(3\kappa + 1)(3\kappa + 4)}$
$a_8 : \frac{6\kappa + 2}{3\kappa + 4}$	$b_8 : \frac{18\kappa^2 - 6\kappa - 22}{(3\kappa + 1)(3\kappa + 4)}$
$a_9 : -\frac{6\kappa + 2}{3\kappa + 4}$	$b_9 : \frac{6\kappa + 2}{3\kappa + 4}$
$a_{10} : 2$	$b_{10} : -\frac{6\kappa + 2}{3\kappa + 4}$
$a_{11} : 2$	$b_{11} : \frac{6\kappa + 2}{3\kappa + 4}$
	$b_{12} : -\frac{18\kappa^2 + 30\kappa - 10}{(3\kappa + 1)(3\kappa + 4)}$
	$b_{13} : -\frac{12}{3\kappa + 4}$
	$b_{14} : -\frac{6\kappa + 2}{3\kappa + 4}$
	$b_{15} : \frac{6\kappa + 2}{3\kappa + 4}$

Figure 1. Model of a Strike-Slip Fault in a Layer Lying Over a Half-Space.

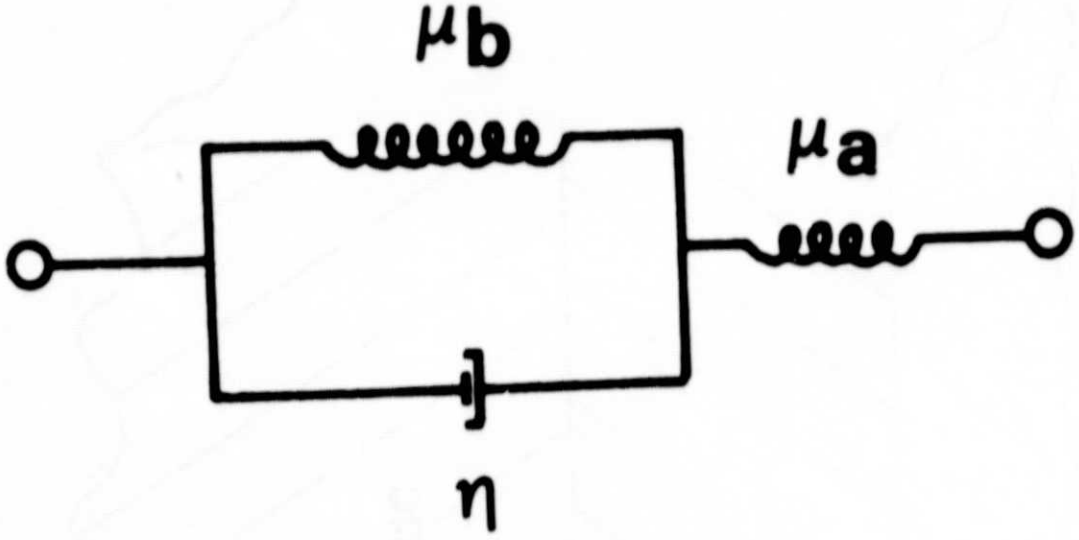

A.

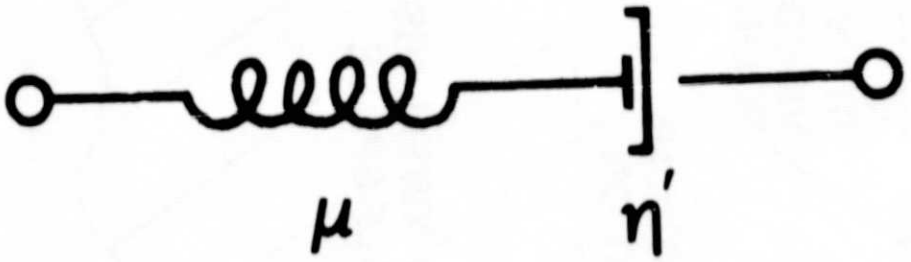

B.

Figure 2. (A) Rheological Element for Standard Viscoelastic Solid. (B) Rheological Element for Maxwell Substance.

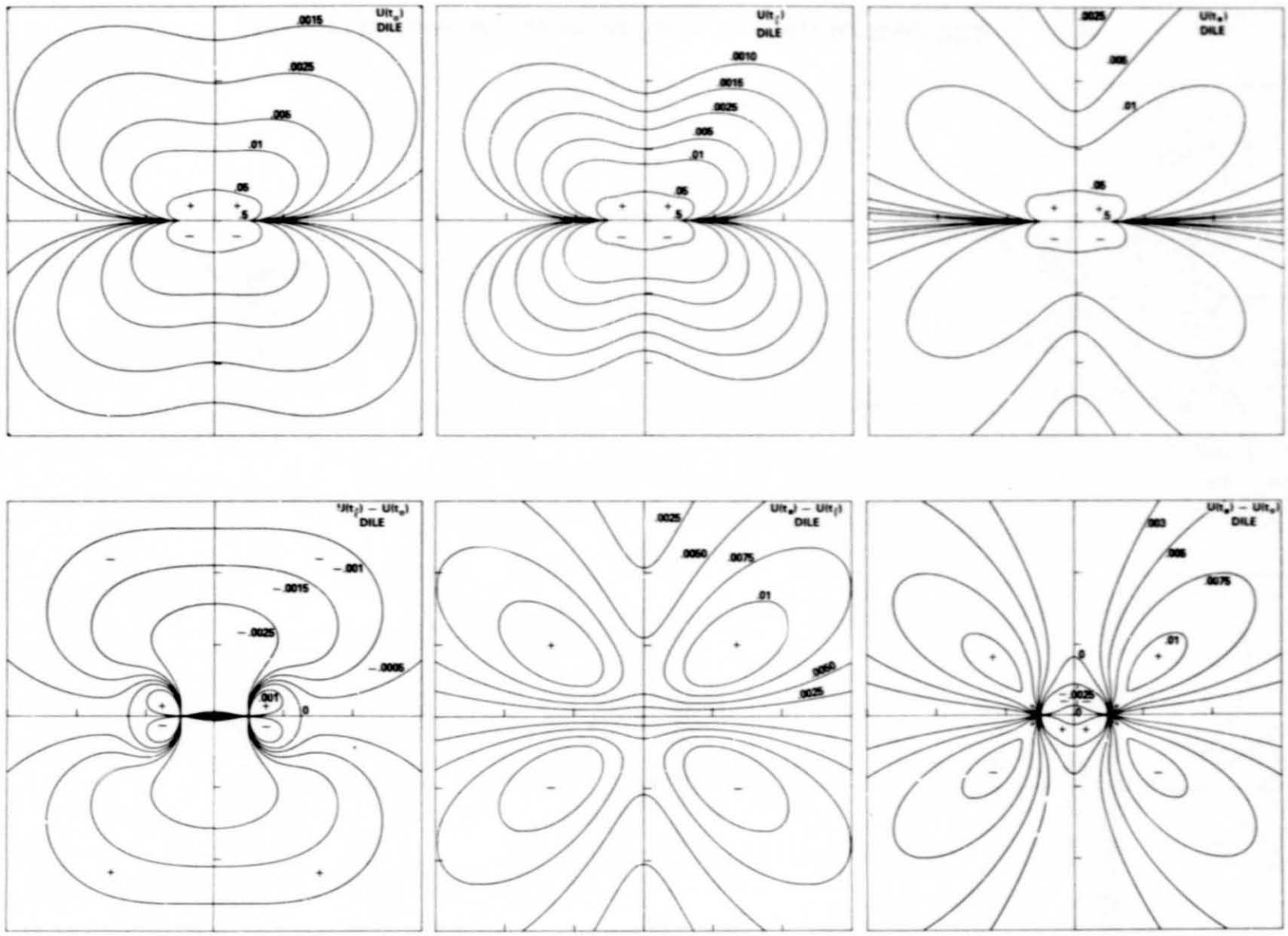

Figure 3. Displacements Parallel to the Fault, u(t), for Model DILE; u_0 = 1 m;
Tick Mark Spacing = 2L

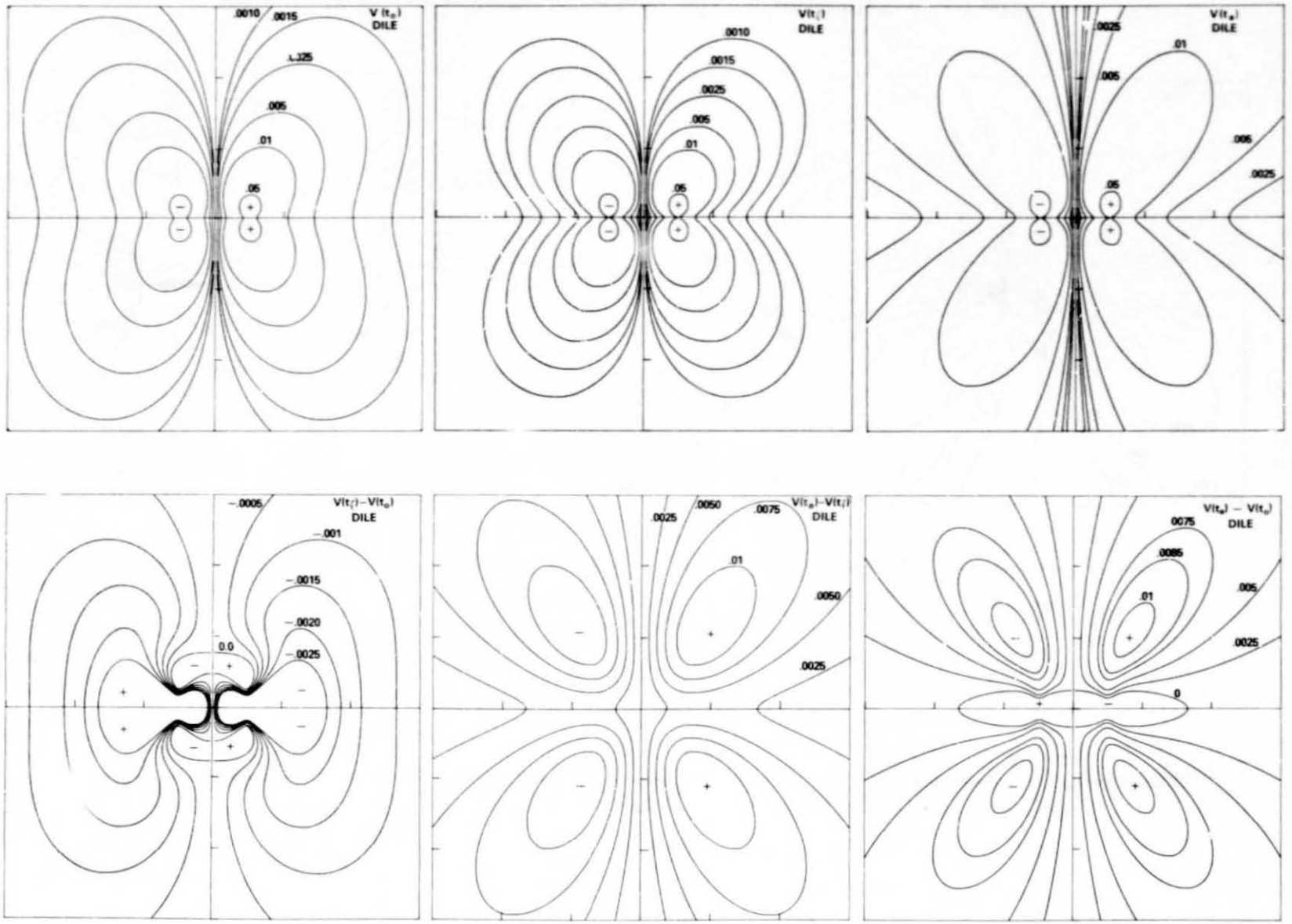

Figure 4. Displacements Perpendicular to the Fault, v(t), for Model DILE; u_0 = 1 m.

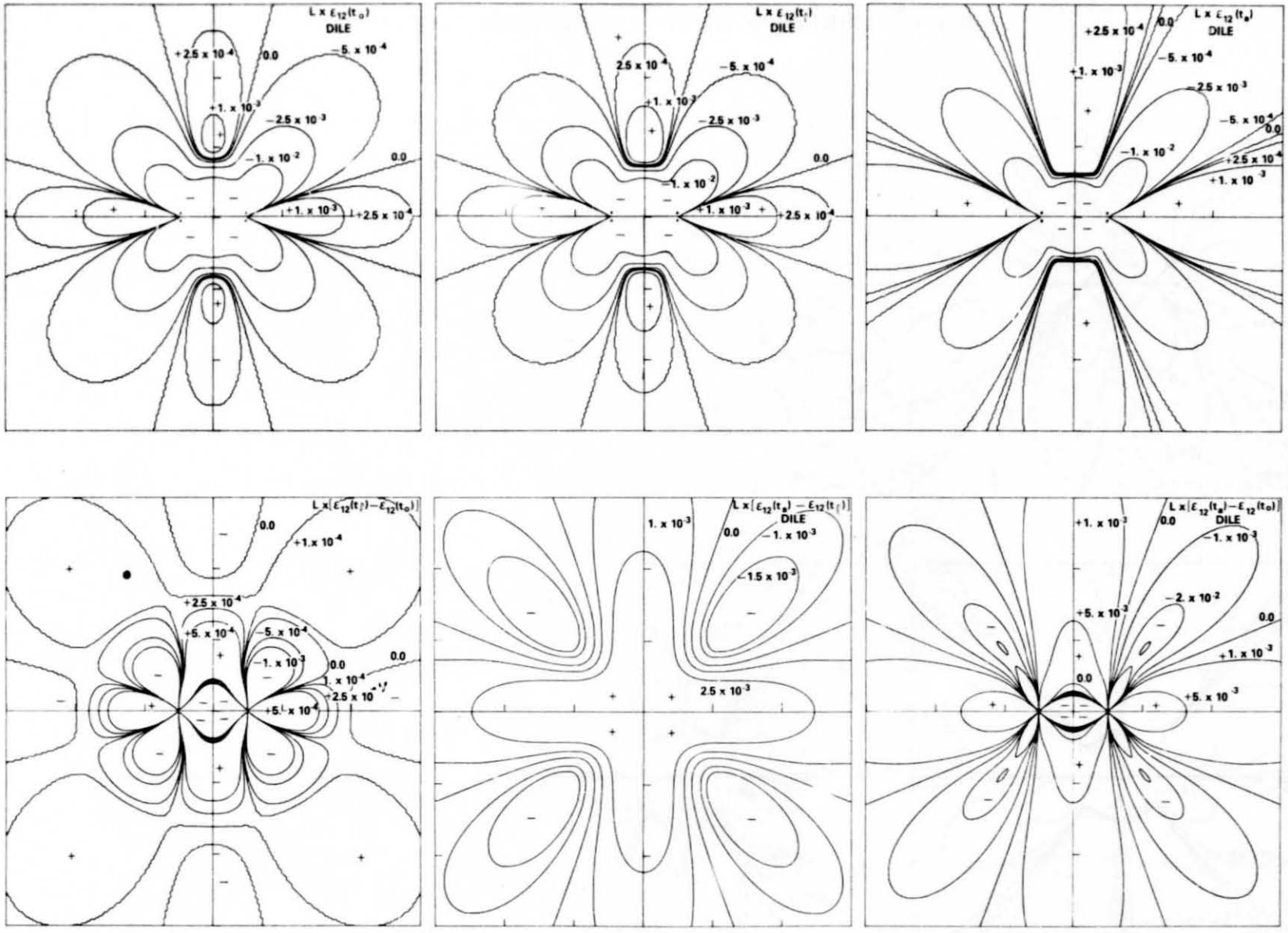

Figure 5. Shear Strain, $\epsilon_{12}(t)$, for Model DILE; u_0 = 1 m.

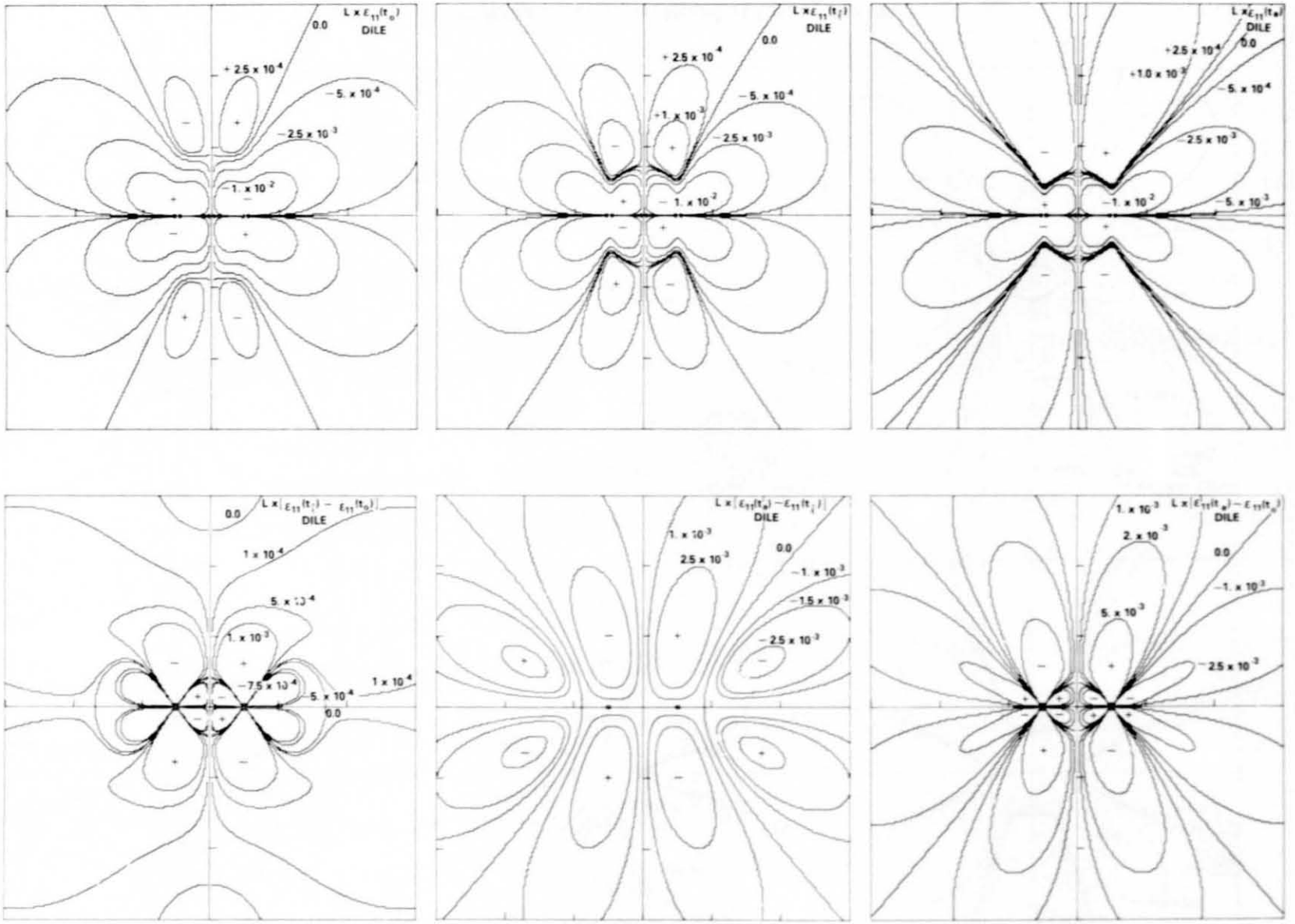

Figure 6. Normal Strain, $\epsilon_{11}(t)$, for Model DILE; u_0 = 1 m.

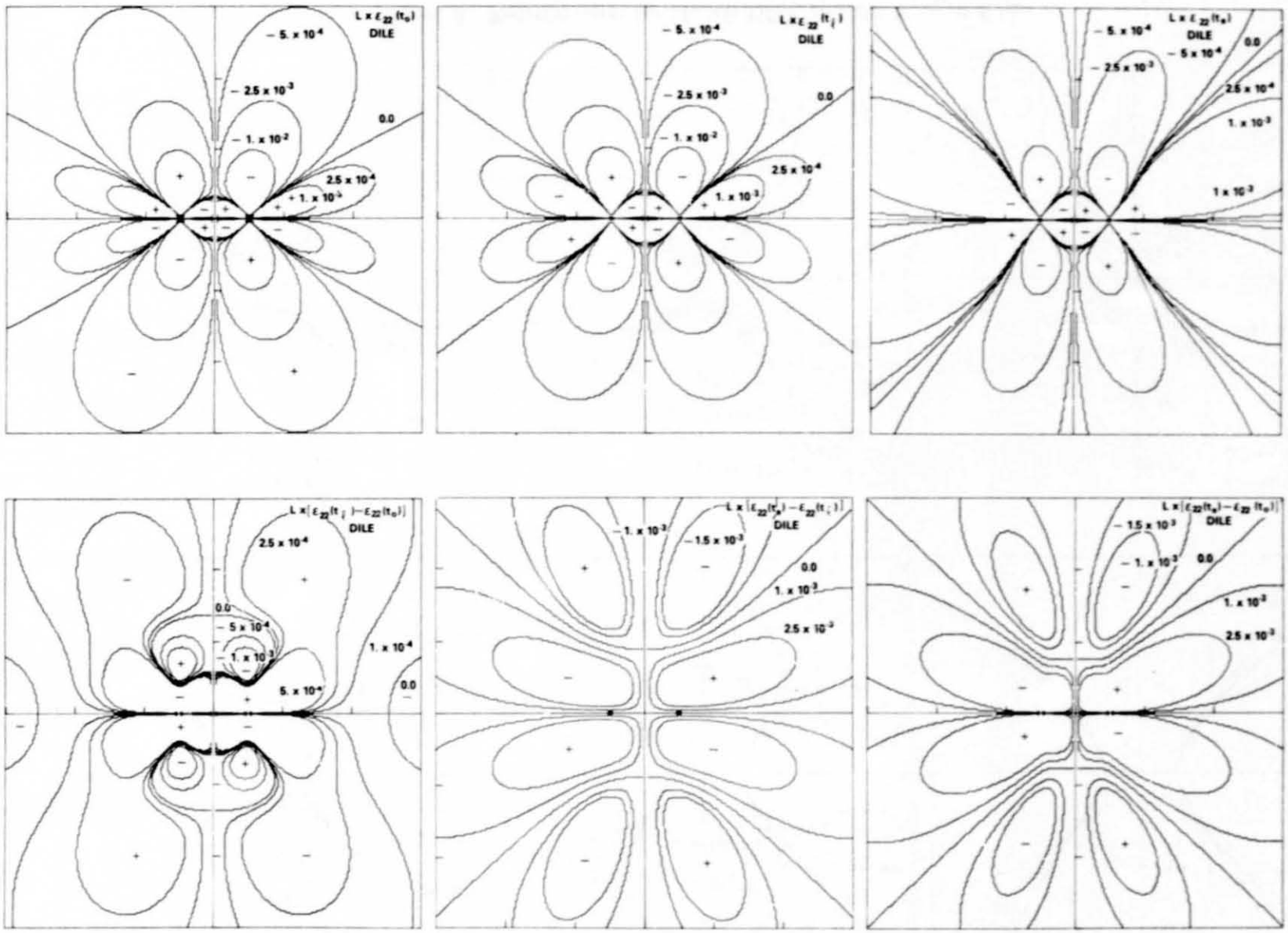

Figure 7. Normal Strain, $\epsilon_{22}(t)$, for Model DILE; u_0 = 1 m.

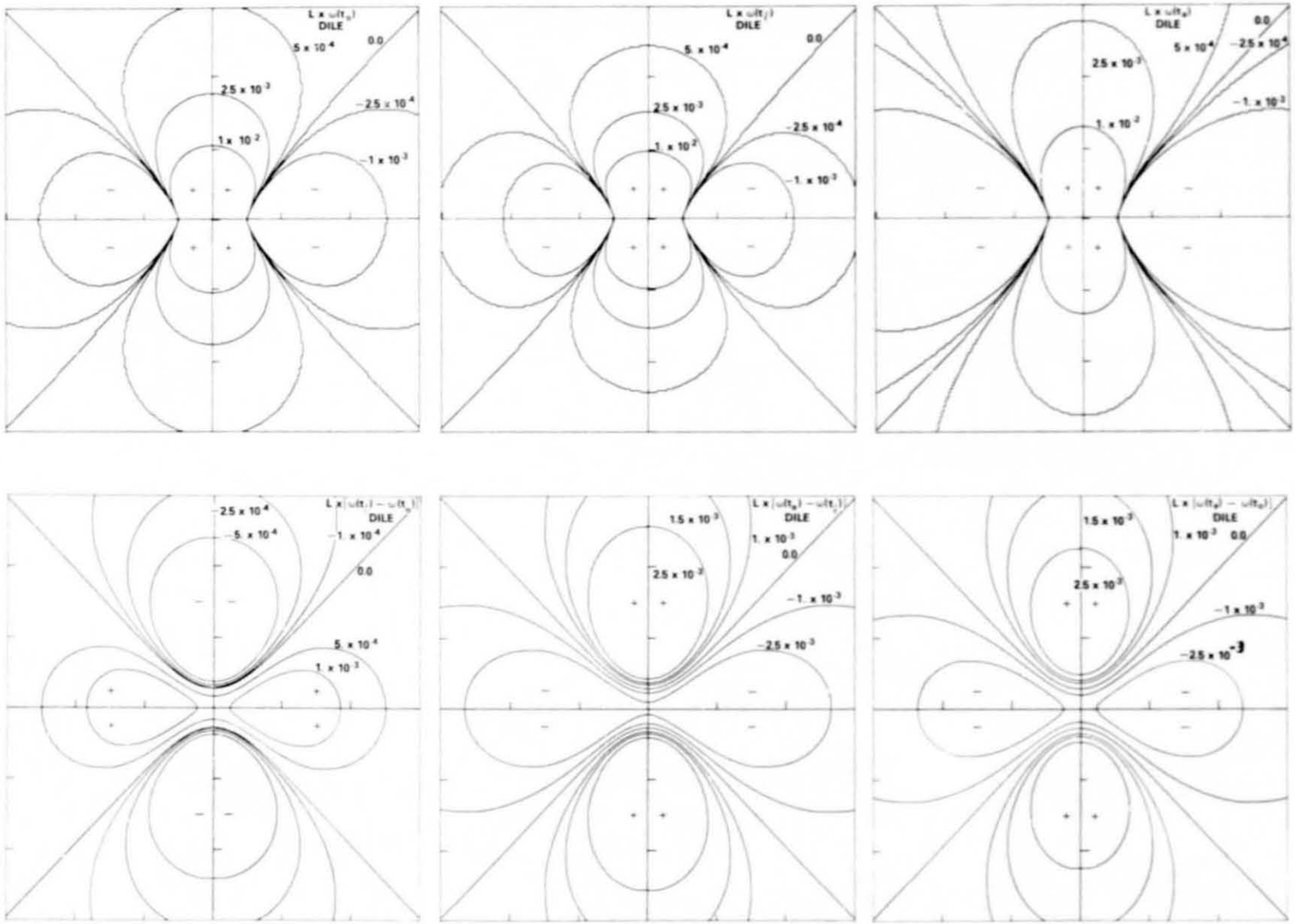

Figure 8. Rotation $\omega(t)$ for Models DILE and DILV; u_0 = 1 m.

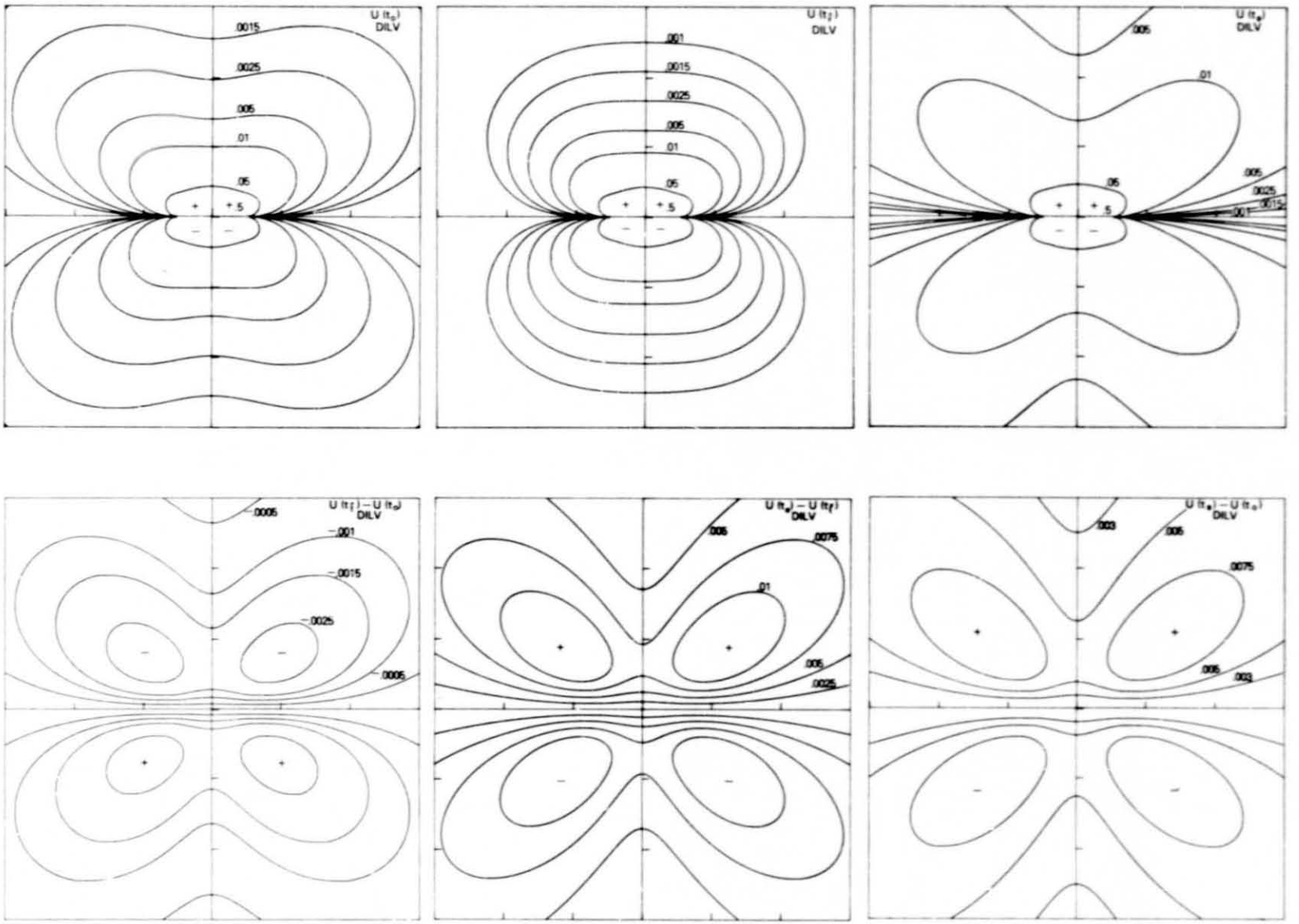

Figure 9. Displacements Parallel to the Fault, u(t), for Model DILV; u_0 = 1 m.

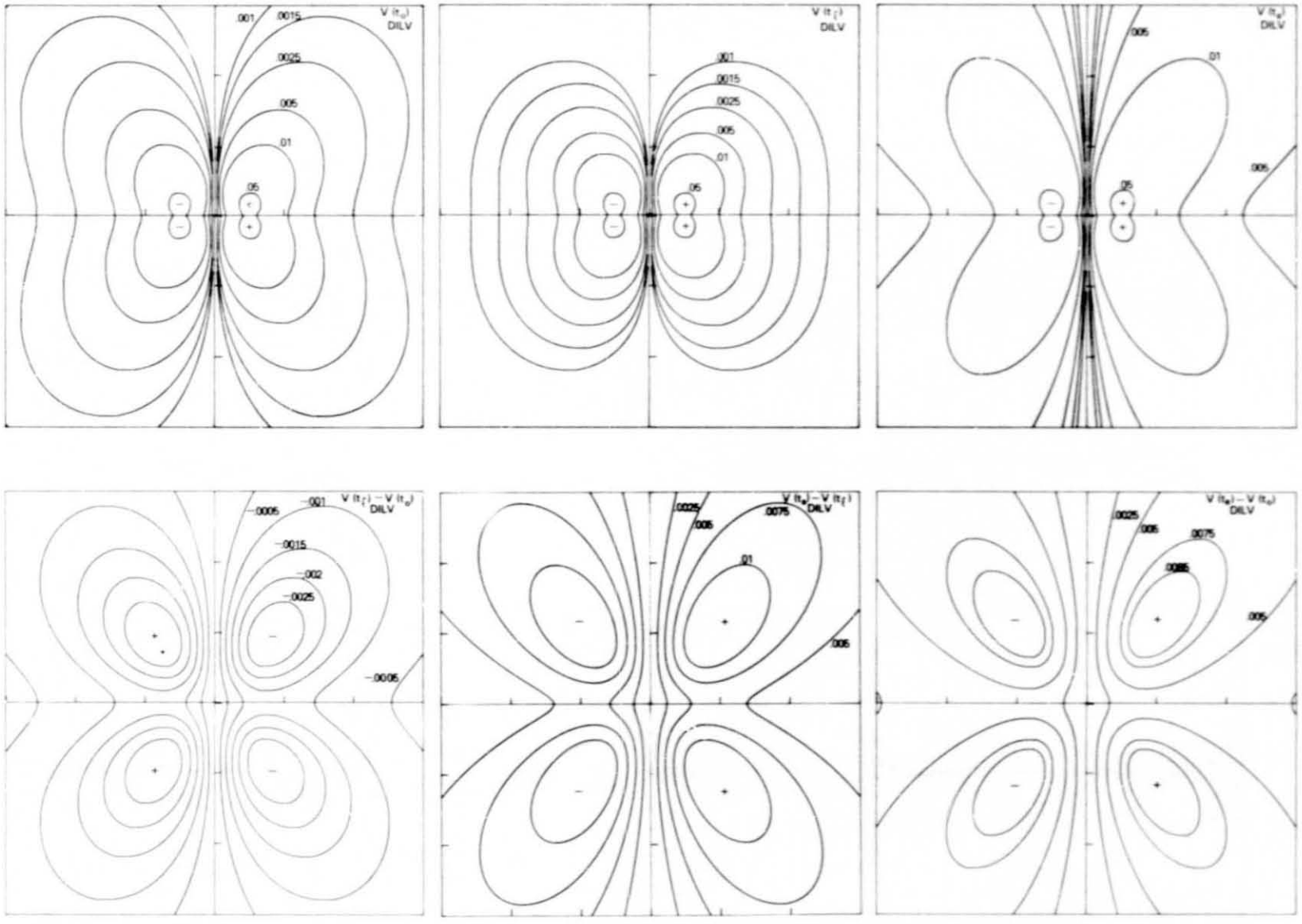

Figure 10. Displacements Perpendicular to the Fault, v(t), for Model DILV; u_0 = 1 m.

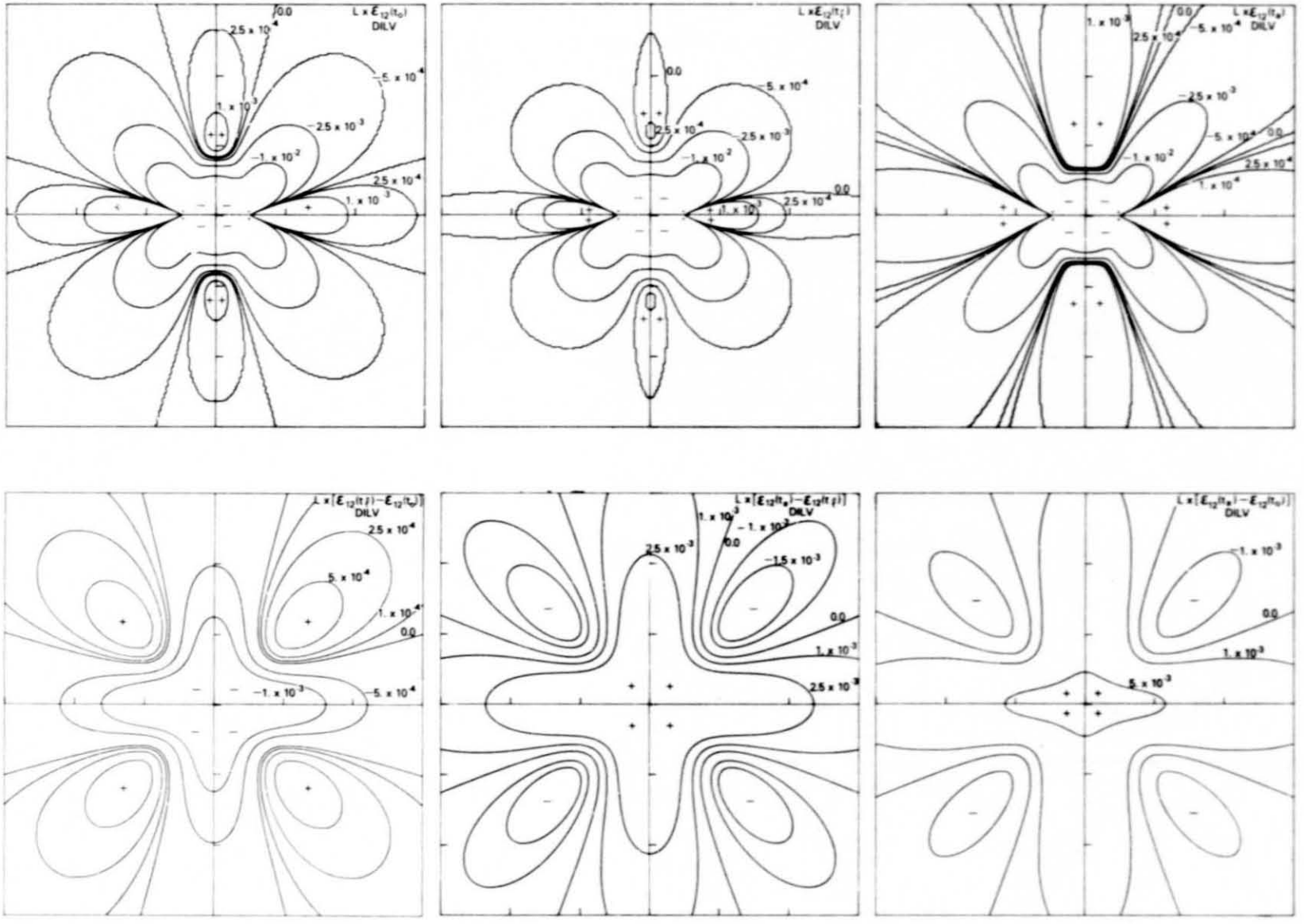

Figure 11. Shear Strain, $\epsilon_{12}(t)$, for Model DILV; u_0 = 1 m.

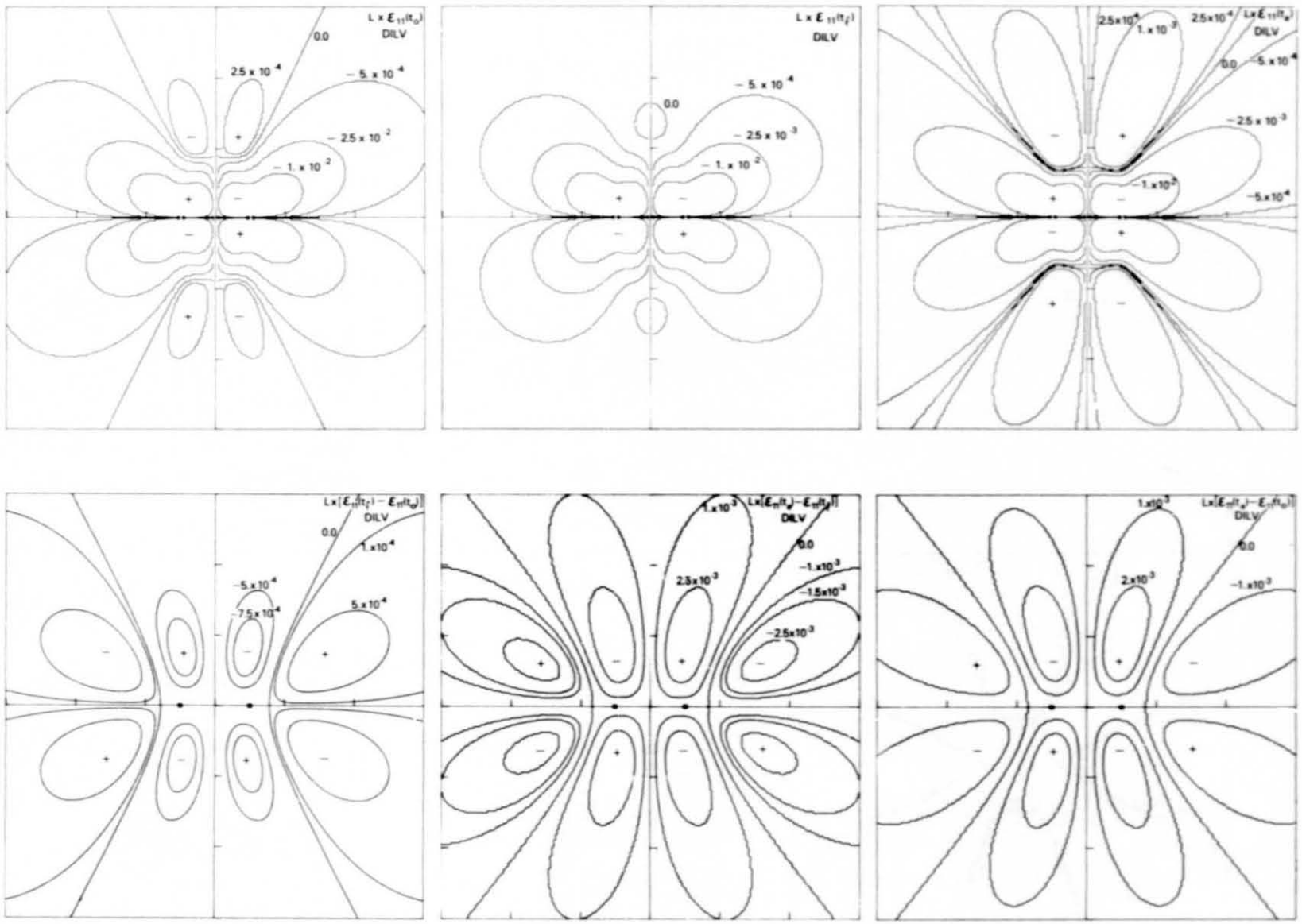

Figure 12. Normal Strain, $\epsilon_{11}(t)$, for Model DILV; u_0 = 1 m.

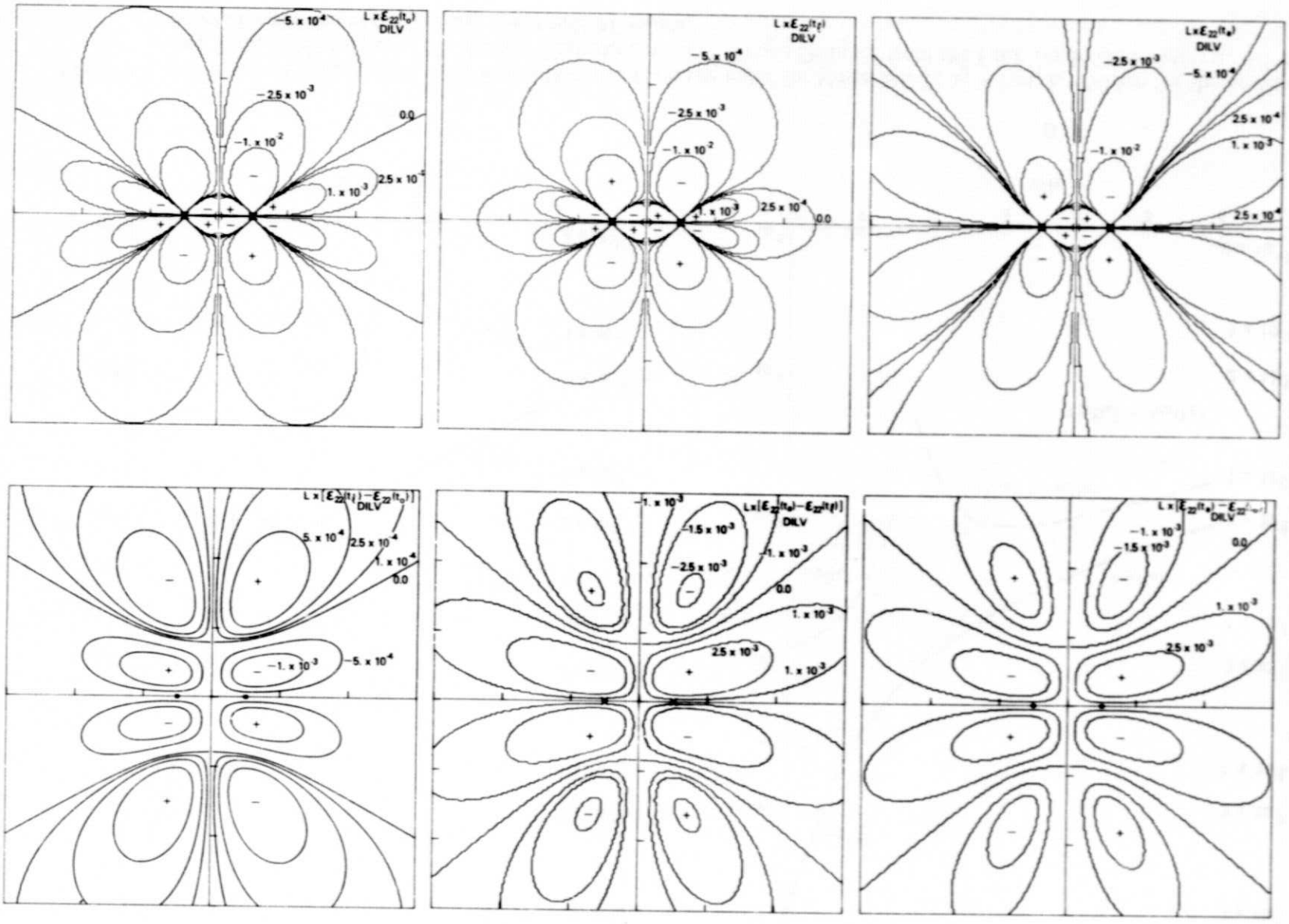

Figure 13. Normal Strain, $\epsilon_{22}(t)$, for Model DILV; u_0 = 1 m.

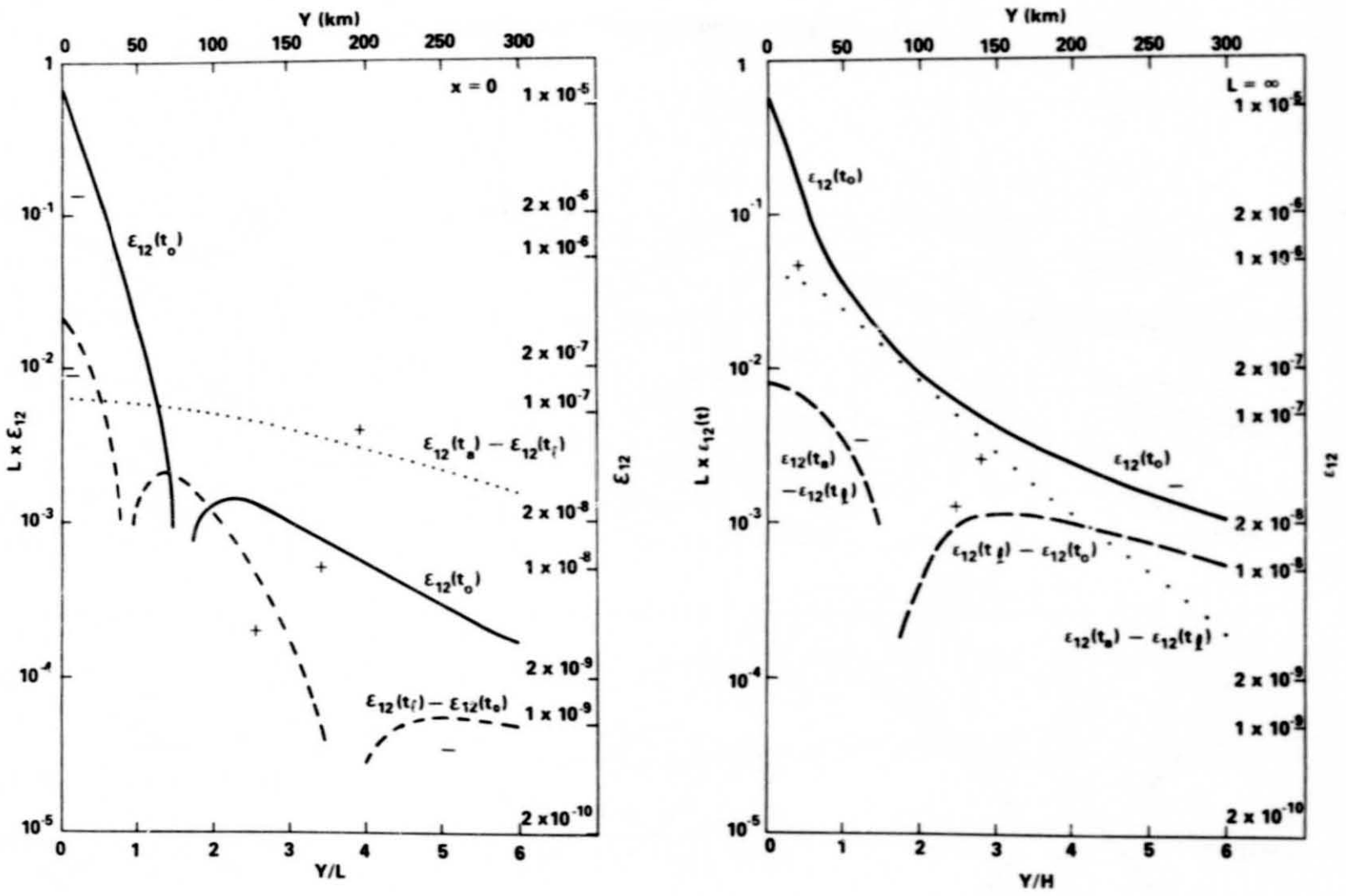

Figure 14. (A) Parallel Displacement, u(t), Versus Distance from the Fault for Model DILE; u_0 = 1 m, L = 50 km for the Scales on Top and Right Side of Figure. (B) Parallel Displacement, u(t), Versus Distance from the Fault for Infinite Fault; u_0 = 1 m, H = 50 km for the Scales on Top and Right Side of Figure.

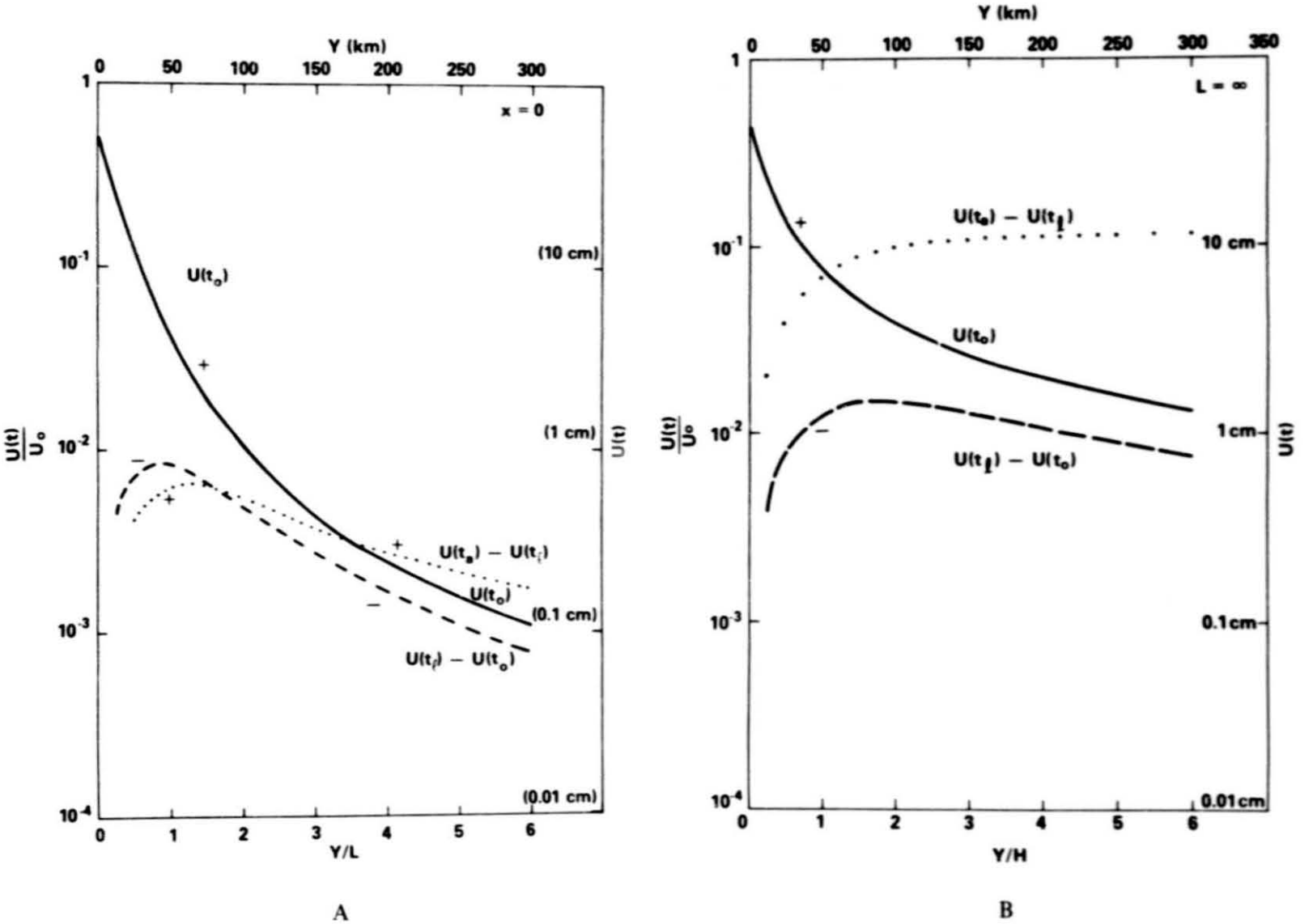

Figure 15. (A) Shear Strain, $\epsilon_{12}(t)$, Versus Distance from the Fault for Model DILE; u_0 = 1 m, L = 50 km for the Scales on Top and Right Side of Figure. (B) Shear Strain, $\epsilon_{12}(t)$, Versus Distance from the Fault for Infinite Fault; u_0 = 1 m, L = 50 km for the Scales on Top and Right Side of Figure.